Biosensors and Bioelectronics 126 (2019) 249–254

Contents lists available at ScienceDirect

Biosensors and Bioelectronics

journal homepage: www.elsevier.com/locate/bios

In-Situ imaging detection of cell membrane and intracellular cholesterol via cascade reactions

Yaqiong Gao[a], Yafeng Wu[a,*], Kaige Zhao[a], Huaisheng Wang[b], Songqin Liu[a]

[a] Jiangsu Engineering Laboratory of Smart Carbon-Rich Materials and Device, School of Chemistry and Chemical Engineering, Southeast University, Nanjing 211189, China
[b] Department of Chemistry, Liaocheng University, Liaocheng, Shandong 252059, China

ARTICLE INFO

Keywords:
In-situ
CL image
Membrane cholesterol
Intracelluar cholesterol

ABSTRACT

Herein, an effective membrane-to-intracellular cholesterol detection strategy was designed based on cascade reactions. A biochip array was firstly fabricated by consecutively immobilizing luminol modified gold nanoparticles (Au@luminol), soybean peroxidase (SBP) and cholesterol oxidase (ChoX) on the cellulose acetate (CA) membrane functionalized home-made micropore array. When cholesterol existed, it was oxidized by ChoX generating H_2O_2, which further triggered the CL reaction under the SBP catalysis, the CL signals were collected by a charge-coupled device (CCD). The proposed strategy exhibited a wide linear range from 0.12 μM to 1000 μM and relatively low detection limit (LOD) of 0.08 μM. Furthermore , it could be used to in-situ detect membrane cholesterol and intracelluar esterified cholesterol in HepG2 cells. After activated HepG2 cells were added to the modified biochip, membrane cholesterol was detected directly. Intracelluar esterified cholesterol was detected through the introduction of triton X-100 and cholesteryl esterase (ChoE). Additionally, the cholesterol content in cells was changed after stimulated by drugs, such as apolipoprotein A-I (ApoA-I), pitavastatin or probucol. The correlation of the CL signal with the amount of cholesterol confirmed that our strategy was feasible to simultaneously detect membrane and intracellular cholesterol at different cellular states. The proposed strategy exhibited excellent sensitivity, selectivity, stability, and reproducibility in a simple, cheap way, which opened a new door for studying clinic treatment of the cholesterol-related diseases.

1. Introduction

Cholesterol is a kind of small lipid molecule which plays an important physiological role in the body. Celluar cholesterol, including membrane cholesterol and intracellular esterified cholesterol, is related to cell survival and various functions of mammalian cells (Ingolfsson et al., 2015; Maxfield and Tabas, 2005). Cholesterol is a main constituent of cell membrane who is essential to maintain membrane structural integrity and fluidity (Kaddah et al., 2018; Morissette et al., 2018). The formation of lipid raft and membrane microstructure domain is partly attributed to cholesterol participation (Lingwood and Kai, 2010). Intracellular cholesterol mainly contributes to the storage of cholesterol in the form of esterified cholesterol (Head et al., 2014; Sonnino and Prinetti, 2013). The regulation of celluar cholesterol keeps cholesterol balance by exporting to plasma lipoproteins or converting into steroids, oxysterols, bile acids, vitamin D3 and other functional derivatives (Bovenga et al., 2015; Das et al., 2014). However, excessive cholesterol intake or cholesterol regulatory mechanism imbalance may lead to some diseases, such as atherosclerosis, Alzheimer's disease or Niemann Pick type C (NPC) (Khera et al., 2011). Since cholesterol plays a vital role in human health, it is required to maintain a stable level precisely. The celluar cholesterol can be excreted with the assistance of apolipoprotein A-I (ApoA-I) or clinic drugs such as pitavastatin and probucol (Rui et al., 2016; Steck and Lange, 2010). As the primary protein component of high density lipoprotein (HDL), ApoA-I is able to bind with ATP-binding cassette transporter A1(ABCA1) specifically, which is an integral membrane protein that mediates the transport of cellular cholesterol (Liu et al., 2014). Pitavastatin is a most recent developed statin drugs who can enhance the expression of ABCA1 to lower lipid, while probucol is a synthetic lipophilic statin who can increase the expression of scavenger receptor class B type I (SR-BI), which is a cell receptor of cholesterol reverse (Hihara et al., 2013; Pirillo and Catapano, 2017). Accordingly, the development of the strategy to sensitively detect celluar cholesterol at different states is very attractive for clinical treatment of cholesterol-relative diseases.

So far, various methods for cholesterol detection have been developed (Zhang et al., 2012; Manjunatha et al., 2012; Rahman et al., 2014; Stewart et al., 2015; Sun et al., 2017; Anirudhan et al., 2018; Satvekar

* Corresponding author.
E-mail address: wuyafeng_1985@163.com (Y. Wu).

https://doi.org/10.1016/j.bios.2018.10.062
Received 13 July 2018; Received in revised form 27 October 2018; Accepted 29 October 2018
Available online 03 November 2018
0956-5663/

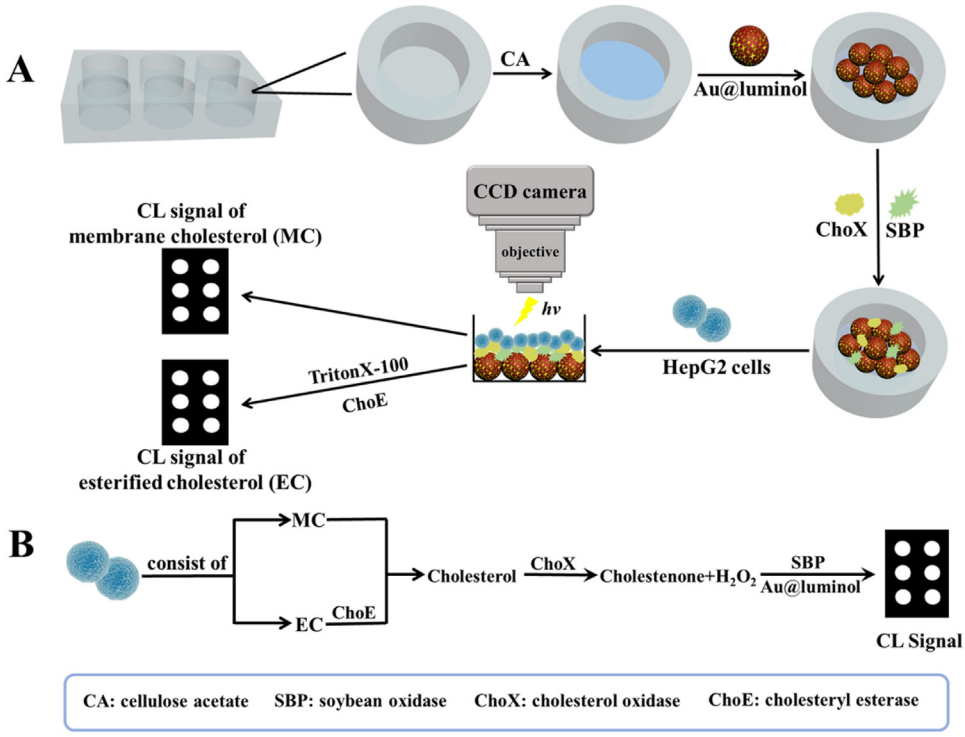

Scheme 1. (A) Schematic preparation process of the CL biochip by immobilization of Au@luminol nanohybrids, SBP and ChoX continuously. CL signals were obtained by CCD. (B) The luminescence mechanism of membrane cholesterol and esterified cholesterol detection via cascade reactions·H_2O_2 produced from cholesterol decomposed by ChoX enzymolysis, then further reacted with Au@luminol under the SBP catalysis to obtain CL signals.

and Pawar, 2018; Wang et al., 2018). For example, Sun et al. used a nitrogen-doped graphene quantum dot/chromium picolinate complex-based sensor to realize fluorescence detection of cholesterol with a detection limit of 0.4 μM (Sun et al., 2017). Zhang et al. (2012) set up a cholesterol biosensor based on luminol electrogenerated chemiluminescence with the linear range from 3.3 μM to 1.0 mM and the detection limit of 1.1 μM (Zhang et al., 2012). Differential pulse voltammetry (DPV) and amperometry were also employed to determine cholesterol in previous studies (Manjunatha et al., 2012; Rahman et al., 2014). However, these reported methods suffered from relatively complex synthesis of materials and high cost of instrument tests. In addition, most studies were limited in serum sample test and only single species sample was allowed to be tested at the same time. To determine cholesterol in cells, high performance liquid chromatography with UV detector was utilized with disrupting cells under ultrasonication and extracting cholesterol from cells using organic solvent, which was quite inconvenient. Therefore, it is still a great challenge to analyse membrane cholesterol and intracellular esterified cholesterol respectively with a simple method.

To avoid the drawbacks of previous reported works, Jiang's group reported a pioneering work about the cholesterol detection at single cells using g-C_3N_4 nanosheets modified with Au NPs/ITO with enhanced electrochemiluminescence (Xu et al., 2017). Inspired by their work, here, we constructed a novel CL biochip to in-situ determine membrane and intracellular cholesterol in HepG2 cells, which was prepared by anchoring Au@luminol nanohybrids, soybean peroxidase (SBP) and cholesterol oxidase (ChoX) successively onto cellulose acetate (CA) membrane modified home-made micropore array. Combining Au NPs and luminol realized luminescent agents immobilization, leading to the enhancement of electron transfer and luminescent intensity (Zhang et al., 2017). SBP is an anionic glycoprotein owning the catalysis capability in luminol-H_2O_2 system with the molecular mass of 37 kDa, which possesses better performance including slower rate of luminescence recession and more attractive stability in wide range of temperature and pH than HRP for amplifying CL intensity in catalysis system (Ivan and Sakharov, 2005). After activated HepG2 cells added to the modified biochip, cell membrane cholesterol decomposed by ChoX into H_2O_2, then CL reaction was triggered under the SBP catalysis. Subsequently with the introduction of triton X-100 and cholesteryl esterase (ChoE), intracellular esterified cholesterol was decomposed into cholesterol and triggered the CL reaction under the SBP catalysis. The CL signals were collected by a charge-coupled device (CCD) during the test. Besides, we also explored the influence of some stimulants on celluar cholesterol. ApoA-I, pitavastatin and probucol were chosen to incubate with HepG2 cells, then membrane and intracellular cholesterol were detected simultaneously as the same way above, which revealed the celluar cholesterol content at different states.

2. Experimental section

2.1. Preparation of the luminol modified Au nanoparticles (Au@luminol)

As shown in Fig. S1, the Au@luminol nanohybrids were prepared by electrostatic interaction according to *Cui's* method with slightly modification (Cui et al., 2017). Briefly, $HAuCl_4$ was reduced by trisodium citrate to obtain AuNPs with diameter of ~13 nm (Hua et al., 2010). The concentration of the resulting Au NPs was 12 nM calculated according to the literature and diluted three times before use (Zhou et al., 2013). Then equal volume Nafion (5% w/w in water and 1-propanol) was mixed with AuNPs solution, then stirred at room temperature for 8 h, centrifuged at 14,000 rpm for 30 min and washed with PBS for three times to get Nafion modified Au nanoparticles (AuNPs/Nafion). 250 μL PDDA (poly(diallyldimethylammonium chloride), 4 wt% in water) was added into 4.75 mL luminol solution (5.26 mM in 0.05 M NaOH) and stirred for 6 h at 60 °C to obtain luminol modified PDDA complexes (PDDA/luminol). Then, the PDDA/luminol was mixed with AuNPs/Nafion and stirred at room temperature overnight. Finally, the luminol modified Au nanoparticles (Au@luminol) was obtained by centrifuging at 1,000 rpm, washed with PBS for several times before redispersed in water to volume of 500 μL for future uses.

2.2. Preparation of the CL biochip and its imaging mechanism

The fabrication procedure of the biochip was shown in Scheme 1A. CA membrane functionalized home-made micropore array were prepared in advance. First, PDMS base stock A was mixed with firming

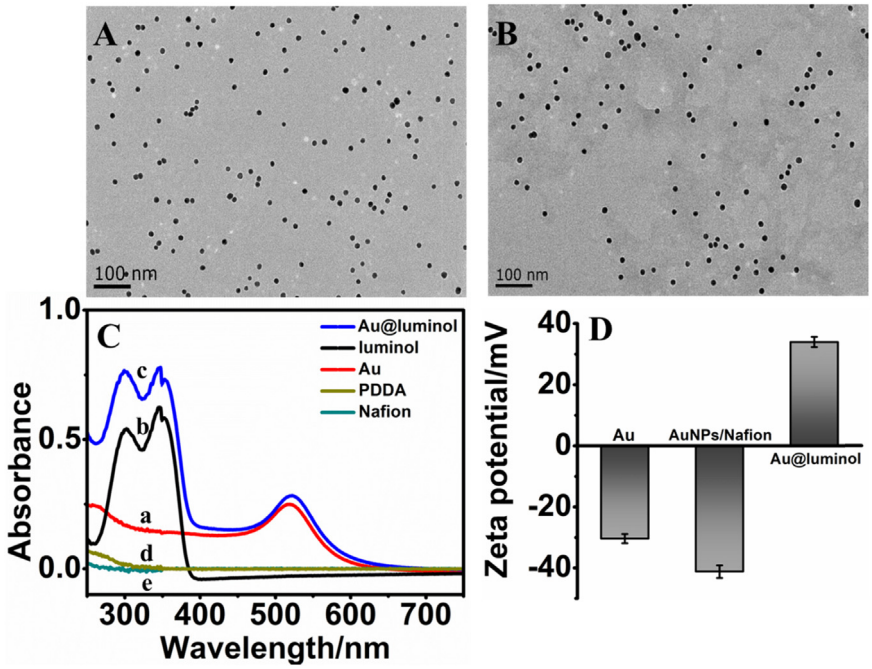

Fig. 1. TEM images of (A) Au NPs and (B) Au@luminol nanohybrids. (C) UV − vis absorption spectra of Au NPs (a), luminol (b), Au@luminol nanohybrids (c), PDDA (d) and Nafion (e). (D) Zeta potential of Au NPs, Au NPs/Nafion and Au@luminol nanohybrids.

agent B at a ratio of 10:1, followed by excluding bubble and puting it into templet before dry out. Second, the PDMS templet was punched with a diameter of 2 mm and depth of 1 mm in 2 × 3 array, which was adhered onto the glass slide for further decoration. Third, 5 μL 2 wt% CA in acetone was added into the micropores and allowed to dry at room temperature for several hours to form CA membrane. Then, 10 μL of Au@luminol nanohybrids were dropped onto the CA membrane and dry at room temperature. This process was repeated three times to ensure sufficient Au@luminol nanohybrids attached on resulting CA membrane. After that, 20 μL SBP (75 U/mL) and ChoX (25 U/mL) were respectively dropped into the micropores and allowed to incubate overnight in the dark at 4 °C followed by washing with PBS (pH 7.4) for three times. Finally, BSA (5% in pH 7.4 PBS) was added into each micropore and incubated for 1 h to reduce background signal. The resulting biochip was washed with PBS and stored in the dark at 4 °C for future uses. 40 μL cholesterol solution with different concentrations were added into the micropores and the CL signals were simultaneously collected by CCD within 50 s exposure time and automatically identified by Acquire Control. The CL signal intensity of each micropore was analyzed and calculated by MetaMorph software. The background from the CCD dark signal was recorded before measurement and subtracted from each images prior to evaluation.

Human blood specimens were received from healthy donors at the Hospital of Southeast University (Nanjing, China). The human blood samples were centrifuged at 2,000 rpm (4 °C) to obtain serum samples before diluting approximately 25 folds with PBS (pH 7.4). After adding 40 μL the serum samples into the micropores array, the CL signals intensities were collected as the same way above.

2.3. The membrane and intracellular cholesterol detection

HepG2 cells were obtained from Shanghai Institute of Biochemistry and Cell Biology of Chinese Academy of Science (Shanghai, China) and seeded in DMEM/high glucose medium supplemented with 10% fetal bovine serum (FBS) and 1% antibiotics (penicillin/streptomycin). Cultures were maintained at 37 °C under a humidified atmosphere containing 5% CO_2.

To detect membrane cholesterol in HepG2 cells, cell membrane needed to be activated by culturing cells in 0.5 mM PBS (pH 7.4) containing 0.31 M of sucrose at 37 °C for 1 h (Ma et al., 2013; Xu et al., 2017). Later, about 2×10^5 activated cells were added into each micropore. As shown in Scheme 1B, the CL signals were collected with the generation of H_2O_2, which was the product of the enzymatic catalyzed reaction between membrane cholesterol and ChoX fixed in CA membrane. After CL signal recording of membrane cholesterol, each micropore was washed with PBS (pH 7.4) for several times, triton X-100 was added to lyse cells. Then, intracelluar esterified cholesterol was hydrolyzed to cholesterol by adding ChoE (15 U/mL), which led to intracelluar cholesterol detection successfully.

To study the impact of different stimulants on cholesterol content, HepG2 cells were incubated with medium containing ApoA-I (10 μg/mL), probucol (50 μM) or pitavastatin (10 μM) for 12 h, respectively. Following the cells were activated and added into the micropores array. Then the CL signals from membrane cholesterol and intracelluar esterified cholesterol were collected as the same way above by CCD and the CL intensities were identified by Acquire Control separately.

3. Results and discussion

3.1. Characterization of Au@luminol nanohybrids

The Au@luminol nanohybrids were synthesized by sequentially assemblying of Nafion and PDDA/luminol onto the surface of AuNPs via electrostatic interaction. The TEM images of Au@luminol nanohybrids showed that the modification of PDDA/luminol did not visibly increase the Au nanoparticles size. Comparing with bare AuNPs, however, the Au@luminol nanohybrids were more dispersive and showed clearly shadow around the spots of AuNPs (Fig. 1A and B). UV–vis spectra showed the characteristic peaks of Au NPs at 522 nm (Fig. 1C, curve a), luminol at 321 nm and 353 nm (Fig. 1C, curve b), respectively. For Au@luminol nanohybrids, the characteristic absorption peaks exhibited the same position as Au NPs and luminol simultaneously (Fig. 1C, curve c), while no obvious absorption peaks were observed for PDDA (Fig. 1C, curve d) and Nafion (Fig. 1C, curve e), confirming that the luminol was successfully coated onto AuNPs. The electrostatic assembly process between AuNPs, Nafion and PDDA/luminol to form Au@luminol

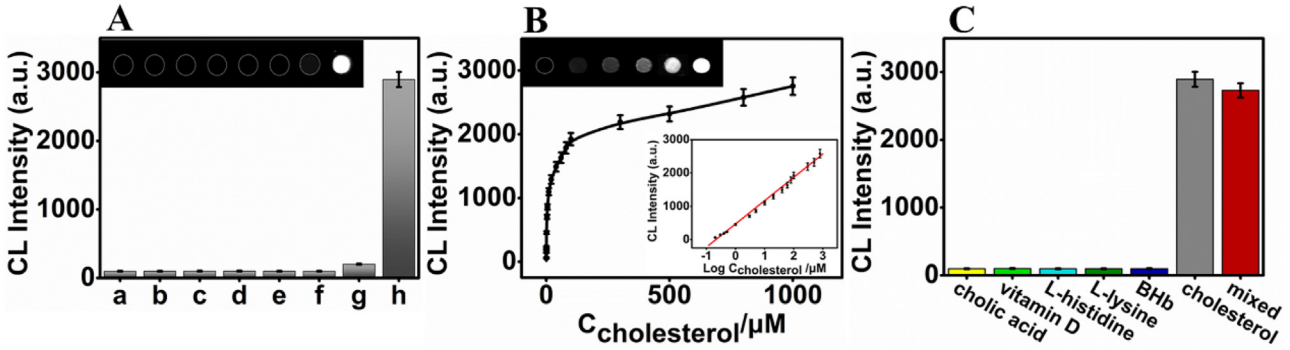

Fig. 2. (A) The CL signals and images of the biochip at different conditions: (a) Au, (b) Au/SBP, (c) Au/ChoX, (d) Au/SBP/ChoX, (e) Au@luminol, (f) Au@luminol/SBP, (g) Au@luminol/ChoX and (h) Au@luminol/SBP/ChoX. The concentration of cholesterol added in each micropore was 1 mM. (B) The variation trend of CL intensity with the increasing concentration of cholesterol solution. The insert graph was the corresponding calibration curve of the biochip with different concentrations of cholesterol from 0.12 μM to 1,000 μM. The insert image was the CL signals images for increasing concentrations of cholesterol solution at 0, 1, 10, 60, 300, 1,000 μM (left to right). (C) The specificity test for the biochip by comparing the CL signal intensity of different solution. The concentration of cholesterol was 1 mM, the concentration of cholic acid, vitamin D, L-histidine, L-lysine, bovine hemoglobin was 56.9 mM.

nanohybrids was confirmed by Zeta potentials measurements. After Nafion coating, the mean Zeta potential of Au NPs was negative shifted from −30.37 mV to −41.21 mV. However, when PDDA/luminol was attached to AuNPs/Nafion, the zeta potential of Au@luminol dramatically changed from −41.21 mV to + 33.97 mV due to the positive surface charged property of PDDA (Fig. 1D). All these observations confirmed the successful assemblage of Au@luminol nanohybrids.

3.2. Construction of the CL biochip

The CL biochip was fabricated by sequentially anchoring of Au@luminol nanohybrids, SBP and ChoX onto CA membrane functionalized home-made micropore array. After addition of cholesterol solution into the micropore, the CL intensity was dramatically increased (Fig. 2A, column h). In the presence of cholesterol, ChoX catalyzed the cholesterol to generate Choleste-4-en-3-one and H_2O_2 (Eq. (1)). Then H_2O_2 reacted with SBP to generate SBP intermediate I (Eq. (2)), which reacted with luminol to form SBP intermediate II and luminol radical (Eq. (3)). The SBP intermediate II was also capable of catalyzing one electron oxidation of luminol to radical product (Eq. (4)). Along with the conversion of the radical product of luminol oxidation into 3-amino-phthalate, powerful CL signal was seized successfully (Eq. (5)).

$$\text{Cholesterol} + O_2 + \text{ChoX} \rightarrow \text{Choleste-4-en-3-one} + H_2O_2 \quad (1)$$

$$\text{SBP} + H_2O_2 \rightarrow \text{SBP intermediate I} + H_2O \quad (2)$$

$$\text{SBP intermediate I} + \text{luminol} \rightarrow \text{SBP intermediate II} + \text{luminol}\bullet \quad (3)$$

$$\text{SBP intermediate II} + \text{luminol} \rightarrow \text{luminol}\bullet + H_2O \quad (4)$$

$$\text{luminol}\bullet \rightarrow \text{3-amino-phthalate} + h\nu \quad (5)$$

Control experiments were performed by modifying CA membrane in micropores with only AuNPs, AuNPs/SBP, AuNPs/ChoX, AuNPs/SBP/ChoX, Au@luminol, Au@luminol/SBP or Au@luminol/ChoX, no CL signal could be observed (Fig. 2A, column a to g). Apparently, luminol was significant luminescent agent to be oxidized and generated CL signal. ChoX acted on cholesterol specifically and engendered H_2O_2 to react with SBP, which was a vital catalyzer for luminol-H_2O_2 CL system according to the "ping-pong" mechanism. Therefore, Au@luminol nanohybrids, SBP and ChoX were essential for biochip construction toward cholesterol determination, which complied with the above mentioned CL mechanism.

The sensitivity of the biochip for cholesterol determination was affected by the loading amount of luminol, SBP and ChoX in each micropore. When the concentrations of luminol used for preparation of PDDA/luminol complex increased from 0 to 5 mM, the CL signal intensity increased gradually (Fig. S2A). Further increasing the luminol concentration led to decrease slightly of CL intensity due to the steric hindrance. Therefore, 5 mM luminol was chosen during the PDDA/luminol preparation.

To verify that SBP possessed better performance than HRP in CL catalysis system, the comparison of catalysis capacity between SBP and HRP was also tested. As shown in Fig. S2B, the CL intensity under the catalysis of SBP was higher than HRP with various exposure time in the biochip, which was consistent with the results that SBP had slower rate of luminescence recession and more attractive stability in our previous work (Liu et al., 2016; Tang et al., 2017). Thus, SBP was chosen to fix into CA of biochip rather than HRP.

Both CL intensities increased with the concentrations of SBP and ChoX during the preparation of biochips. When the concentrations of SBP and ChoX increased to 75 U/mL and 25 U/mL, the CL intensities reached their highest values respectively and became stationary gradually at their higher concentrations. So 75 U/mL SBP and 25 U/mL ChoX were selected as the best concentrations for biochip construction (Fig. S2C and D).

Under the optimum amount of enzymes and luminol in Au@luminol nanohybrids, the CL response intensity also depended on the exposure time for cholesterol determination with CCD. With the exposure time performed from 0 to 50 s, the CL intensity increased to maximum gently. Further prolonging the exposure time led to a decrease of the CL intensity (Fig. S2E). Finally the exposure time of 50 s was used throughout the test. The fluctuation of the CL intensity in pace with exposure time might caused by the decomposing and catalyzing procedure of enzymes to their substrates and the decay of the luminol excited state with the time expanding (Ivan and Sakharov, 2005).

3.3. Cholesterol determination in solution based on the CL biochip

Under the optimal conditions, the CL intensity increased with the increasing of cholesterol concentrations from 0 to 1,000 μM (Fig. S3). The variation of CL intensities were linearly proportional to the logarithm of the concentrations of cholesterol in the range from 0.12 to 1,000 μM, which encompassed over three orders of magnitude (Fig. 2B). The insert CL image in Fig. 2B also exhibited intuitively that the spots lighted gradually when cholesterol concentrations increased. The regression equation was $\Delta CL = 471.18 + 698.43 \log(c_{cholesterol/\mu M})$, with a correlation coefficient of 0.989 and a detection limit (LOD) of 0.08 μM (S/N = 3). The LOD and linear range for cholesterol detection with the proposed CL biochips were compared with previously reported methods, which was summarized in Table S1. Besides, the biochips consumed minor samples and short time under a simple and fast manipulation, realizing convenient multi-sample detection

simultaneously.

To evaluate the specificity of the proposed biochip, several experiments were conducted to test whether other proteins or lipoid substances could interfere with the cholesterol determination. In this case, the concentration of interferents (cholic acid, vitamin D, L-histidine, L-lysine and bovine hemoglobin) was 56.9 mM, which was 10 times higher than the pathophysiological concentration. No remarkable CL signals were observed from the interferents, attesting the proposed biochips had no obvious cross-reactivity and nonspecific binding (Fig. 2C).

To demonstrate the accuracy of the proposed detection strategy, cholesterol in human serum samples were tested by comparing the results obtained from the prepared biochip with commercial ELISA kit test. As the cholesterol concentration in human serum samples from healthy donors at the Hospital of Southeast University were over the calibration ranges, serum samples were diluted before test. The concentration of cholesterol in serum samples detected by the prepared CL biochips to be 97.187 μM, 115.760 μM and 105.952 μM respectively, which was in the scope of cholesterol content in healthy human serum. The results indicated that the proposed method was able to detect cholesterol in plasma at the entire range of pathophysiology with proper dilution (Table 1). Recovery experiments were carried out by adding known amount of cholesterol to the real samples. The recoveries of the human serum samples ranged from 94.1% to 104.6% with the RSD less than 3.6%, indicating the proposed biochips were reliable for the cholesterol determination in real samples. The relative percentage error obtained from the two methods was less than 2.4%, which indicated the accuracy of the proposed method. The CL images of human serum samples and recovery samples were exhibited in Fig. S5.

The reproducibility of the biochip was also examined by using five biochips fabricated independently. The maximum relative standard deviation (RSD) was 5.4%. When a same biochip was used to test repetitively in five micropores at same concentration of cholesterol (500 μM), the RSD was < 4.5% (Fig. S5A). Thus, the proposed biochips possessed a relative good detection reproducibility and precision. When the as-prepared biochips were stored in the dark at 4 °C for 4 weeks, the CL signal intensity were not decline significantly, whose recovery reached 97.4% from the beginning signal intensity for cholesterol determination (Fig. S5B). Therefore, the prepared biochip possessed favourable storage stability.

3.4. Determination of membrane and intracellular cholesterol in HepG2 cells

To test the membrane and intracellular cholesterol, activated HepG2 cells were added into the prepared biochip, membrane cholesterol reacted with ChoX to generate H_2O_2, which triggered the CL reaction of luminol under the catalysis of SBP (Scheme 1B). The amount of membrane cholesterol of 2×10^5 activated cells was detected to be 1.31 ± 0.03 μM, which was about $(1.58 \pm 0.04) \times 10^8$ cholesterol molecules in each HepG2 cell membrane. The relative standard deviation (RSD) for five times repeatedly detecting in the same biochip was calculated to be < 4.6% (Fig. S6A) and the CL intensities and images were exhibited in Fig. S6B. Afterwards, HepG2 cells were lysed by tritonX-100 to expose the intracelluar esterified cholesterol, which could be decomposed into cholesterol by ChoE. To ensure the intracellular esterified cholesterol decomposed by ChoE completely, the amount of ChoE introduced into the micropores after lysis by tritonX-100 was optimized. When the amount of ChoE was increased to 15 U/mL, the CL intensity attained highest value and flattened out with further rising ChoE concentrations, indicating that 15 U/mL of ChoE was enough to resolve intracellular esterified cholesterol (Fig. S1F). Thus 15 U/mL ChoE was employed during the intracelluar esterified cholesterol detection. The intracelluar cholesterol was analyzed to be 0.88 ± 0.02 μM for 2×10^5 cells according to the proposed biochip, which evaluated about $(1.06 \pm 0.02) \times 10^8$ molecules as intracelluar cholesterol presented in each HepG2 cell. The relative standard deviation (RSD) for five times repeatedly detecting in the same biochip was calculated to be < 4.3% (Fig. S6A) and the CL signal intensity and image were exhibited in Fig. S6C. The monitored cholesterol both free doped in cell membrane and esterified cholesterol in interior of HepG2 cells were in accord with the literature results approximately (Ma et al., 2013; Xu et al., 2017), confirming the accuracy of the proposed method.

Many diseases are caused by abnormal cholesterol metabolism or excessive cholesterol intake, which requires more attention to study for regulating cholesterol balance (Mazidi et al., 2017). ApoA-I, pitavastatin and probucol were effective components to depress the cholesterol level. To study the capability of ApoA-1, pitavastatin and probucol to effuse cholesterol from cells respectively, different concentrations of ApoA-I, pitavastatin and probucol were incubated with cells for various period. The celluar cholesterol performed varying degrees of decline trend, exhibiting the CL intensity decreased gradually with increscent concentrations within a certain range under the stimulants above. When the concentrations of ApoA-I, pitavastatin and probucol reached 10 μg/mL, 10 μM and 50 μM respectively, the differences of the CL intensities (ΔCL, the difference of CL intensity before and after stimulated by ApoA-I, probucol or pitavastatin) were maximum. Further increasing of the concentrations of all three stimulants led to ΔCL stabilization (Fig. 3A–C). With the prolongation of incubation time, ΔCL caused by ApoA-I, pitavastatin and probucol all reached their maximum values at 12 h (Fig. 3D). Therefore 10 μg/mL ApoA-I, 10 μM pitavastatin and 50 μM probucol were decided to incubated with HepG2 cells for 12 h respectively. As shown in Fig. S7A, at the optimal conditions of concentrations of the three stimulants and incubating time, the ΔCL of membrane and intracelluar cholesterol under the stimulation of ApoA-I was highest while probucol was lowest, which approved the capability of ApoA-I to transport celluar cholesterol is greater than pitavastatin and probucol (Gao et al., 2017; Maejima et al., 2011). After treatment of 2×10^5 cells with ApoA-I (10 μg/mL), pitavastatin (10 μM) and probucol (50 μM) for 12 h, the membrane cholesterol decreased to ~1.18 μM for ApoA-I, ~1.21 μM for pitavastatin and ~1.27 μM for probucol respectively. It was evaluated that $\sim 1.56 \times 10^7$, $\sim 1.21 \times 10^7$ and $\sim 0.48 \times 10^7$ cholesterol molecules in each cell membrane were transfered after ApoA-I, pitavastatin and probucol treated, respectively. Meanwhile, intracelluar cholesterol reached ~0.81 μM for ApoA-I, ~0.84 μM for pitavastatin and ~0.86 μM for probucol, evaluated about $\sim 0.84 \times 10^7$, $\sim 0.48 \times 10^7$ and $\sim 0.24 \times 10^7$ cholesterol molecule cells were transferred from intracelluar by ApoA-I, pitavastatin and probucol respectively. The RSD of cholesterol test in membrane incubated with ApoA-I, pitavastatin and probucol were 3.16%, 4.44% and 3.81%, while intracelluar cholesterol test were 2.57%, 2.81% and 3.66%, respectively (Fig. S7B). The results indicated that the test for cell

Table 1
Human serum samples test using the proposed method and commercial methods.

Sample	Added (μM)	Found (μM)	Recovery (%)	RSD (%, n = 3)	Commercial ELISA (μM)	RSD (%, n = 3)
1	0.0	97.2	—	2.6	99.3	2.2
	20.0	116.4	96.0	2.8	118.1	1.5
	50.0	149.4	104.6	2.6	151.1	1.1
	100.0	194.7	97.6	2.0	193.3	− 0.7
2	0.0	115.8	—	1.6	114.8	− 0.8
	20.0	134.8	95.4	3.6	137.7	2.1
	50.0	164.7	97.9	3.2	162.5	− 1.3
	100.0	212.1	96.4	1.9	214.7	1.2
3	0.0	105.9	—	2.1	108.4	2.3
	20.0	125.3	96.8	1.7	127.3	1.6
	50.0	155.3	98.7	2.3	158.1	1.8
	100.0	200. 1	94.1	1.3	203.8	1.9

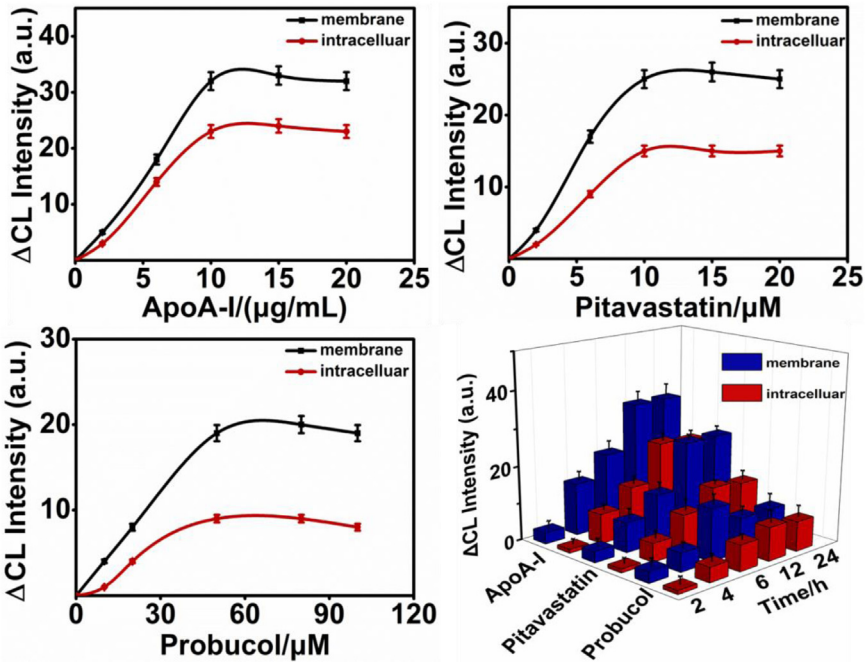

Fig. 3. The ΔCL intensity of membrane and intracelluar cholesterol of HepG2 cells after incubated with various concentrations of ApoA-I (A), pitavastatin (B), probucol (C) and the same stimulants at optimal concentration with different incubating time respectively (D). The ΔCL intensity was the difference of CL intensity before and after stimulated by ApoA-I, probucol or pitavastatin.

population was credible and the downtrend of celluar cholesterol quantity after stimulations of ApoA-I, pitavastatin and probucol was in keeping with the property of them according to the pertinent literature (Maejima et al., 2011; Xu et al., 2017; Zhang et al., 2016).

4. Conclusions

In summary, in-situ imaging detection strategy of cell membrane and intracellular cholesterol via cascade reactions was successfully proposed. Au@luminol nanohybrids were employed to realize luminescent agent immobilization and signal amplification. The ChoX embedded in the CA membrane reacted with the cholesterol specifically, inducing the CL signal under the catalysis of SBP. The proposed biochip was confirmed to detect cholesterol in human serum samples with a wide linear range and relatively low LOD, which could also in-situ detect cell membrane and intracelluar cholesterol, respectively. Besides, cell membrane and intracelluar cholesterol at different cellular states were evaluated, which was accomplished by stimulating cells with ApoA-I, pitavastatin or probucol. As expected, the biochip possessed the advantages of simple operation, minor sample consumption, good reproducibility, acceptable selectivity and accuracy. The proposed strategy showed a promising potential application in cholesterol detection and correlative disease diagnosis.

Acknowledgments

This work was supported by the National Natural Science Foundation of China (No. 21635004, 21627806, 21705018), the Fundamental Research Funds for the Central Universities (2242017K3DN11)

Appendix A. Supporting information

Supplementary data associated with this article can be found in the online version at doi:10.1016/j.bios.2018.10.062.

References

Anirudhan, T.S., Deepa, J.R., Binussreejayan, 2018. Mater. Sci. Eng. C 92, 942–956.
Bovenga, F., Sabbà, C., Moschetta, A., 2015. Cell Metab. 21, 517–526.
Cui, C., Chen, Y., Jiang, D., Zhu, J.J., Chen, H.Y., 2017. Anal. Chem. 89, 2418–2423.
Das, A., Brown, M.S., Anderson, D.D., Goldstein, J.L., Radhakrishnan, A., 2014. Elife 3, e02882.
Gao, X., Li, Y., Jiang, Z., 2017. Drug Des. Dev. Ther. 11, 617–627.
Head, B.P., Patel, H.H., Insel, P.A., 2014. BBA - Biomembr. 1838, 532–545.
Hihara, T., Taniguchi, T., Ueda, M., Yoshinaga, T., Miyamoto, N., Sawada, K., 2013. Hum. Exp. Toxicol. 32, 1028–1037.
Hua, C.P., Wei, W.D., Duan, C.F., Dong, Y.P., Guo, J.Z., 2010. Chem. Eur. J. 13, 6975–6984.
Ingolfsson, H.I., Tieleman, P., Marrink, S., 2015. J. Am. Chem. Soc. 136, 14554–14559.
Ivan, Yu, Sakharov, §, 2005. J. Agric. Food Chem. 53, 5784–5788.
Kaddah, S., Khreich, N., Kaddah, F., Charcosset, C., Greige-Gerges, H., 2018. Food Chem. Toxicol. 113, 40–48.
Khera, A.V., Cuchel, M., Lleramoya, M.D.L., Rodrigues, A., Burke, M.F., Jafri, K., French, B.C., Phillips, J.A., Mucksavage, M.L., Wilensky, R.L., 2011. N. Engl. J. Med. 54, 280–281.
Lingwood, D., Kai, S., 2010. Science 327, 46–50.
Liu, A., Zhao, F., Zhao, Y., Shangguan, L., Liu, S., 2016. Biosens. Bioelectron. 81, 97–102.
Liu, W., Qin, L., Yu, H., Lv, F., Wang, Y., 2014. J. Gastroen. Hepatol. 29, 614–622.
Ma, G., Zhou, J., Tian, C., Jiang, D., Fang, D., Chen, H., 2013. Anal. Chem. 85, 3912–3917.
Maejima, T., Sugano, T., Yamazaki, H., Yoshinaka, Y., Doi, T., Tanabe, S., Nishimakimogami, T., 2011. J. Pharm. Sci. 116, 107–115.
Manjunatha, R., Suresh, G.S., Melo, J.S., D'Souza, S.F., 2012. Talanta 99, 302–309.
Maxfield, F.R., Tabas, I., 2005. Nature 438, 612–621.
Mazidi, M., Gao, H.K., Vatanparast, H., Kengne, A.P., 2017. Medicine 96, e5736.
Morissette, M., Morin, N., Rouillard, C., Di, T.P., 2018. Neuropharmacology 133, 289–306.
Pirillo, A., Catapano, A.L., 2017. Atheroscler. Supp. 27, E1–E9.
Rahman, M.M., Li, X.B., Kim, J., Lim, B.O., Ahammad, A.J.S., Lee, J.J., 2014. Sens. Actuat. B 202, 536–542.
Rui, K., Dan, L., Chen, Y.E., Moon, J.J., Schwendeman, A., 2016. ACS Nano 10, 3015.
Satvekar, R.K., Pawar, S.H., 2018. J. Med. Eng. Technol. 1–9.
Sonnino, S., Prinetti, A., 2013. Curr. Med. Chem. 20, 4–21.
Steck, T.L., Lange, Y., 2010. Trends Cell Biol. 20, 680–687.
Sun, L., Li, S., Ding, W., Yao, Y., Yang, X., Yao, C., 2017. J. Mater. Chem. B 9006–9014.
Stewart, A.J., O'Reilly, E.J., Moriarty, R.D., Bertoncello, P., Keyes, T.E., Forster, R.J., Dennany, L., 2015. Electrochim. Acta 157, 8–14.
Tang, M., Zhou, Z., Shangguan, L., Zhao, F., Liu, S., 2017. Talanta 180, 47–53.
Wang, K., Ren, H., Li, N., Tan, X., Dang, F., 2018. Talanta 188, 708–713.
Xu, J., Jiang, D., Qin, Y., Xia, J., Jiang, D., Chen, H.Y., 2017. Anal. Chem. 89, 2216–2220.
Zhang, A., Guo, W., Ke, H., Zhang, X., Zhang, H., Huang, C., Yang, D., Jia, N., Cui, D., 2017. Biosens. Bioelectron. 101, 219–226.
Zhang, M., Li, L., Xie, W., Wu, J.F., Yao, F., Tan, Y.L., Xia, X.D., Liu, X.Y., Liu, D., Lan, G., 2016. Atherosclerosis 248, 149–159.
Zhang, M., Yuan, R., Chai, Y., Chen, S., Zhong, H., Wang, C., Cheng, Y., 2012. Biosens. Bioelectron. 32, 288–292.
Zhou, Z., Wei, W., Zhang, Y., Liu, S., 2013. J. Mater. Chem. B 1, 2851–2858.